Experimental Comparison of Carbon and Beryllium as Divertor Target Materials in JET

D J Campbell and the JETTeam

JET Joint Undertaking, Abingdon, Oxon OX14 1XA, UK

ABSTRACT

The performance of carbon (CFC) and beryllium as divertor target materials has been investigated in the JET Pumped Divertor under a wide range of experimental conditions. In general, the characteristics of L and H-mode plasmas on the two targets were very similar. In addition, the impurity content in the two cases was similar, and it is believed that carbon sputtered from plasma-facing components in the main chamber played a significant role in beryllium target experiments. The success of the target design was confirmed by the absence of carbon blooms and beryllium melting on tile edges. However, in a specific melt experiment designed to assess the behaviour of plasmas on molten and melted beryllium, little evidence of vapour shielding of the target was found and melt damage to a depth of 3mm was observed.

1. INTRODUCTION

Carbon fibre composites (CFC) and beryllium have been considered as power handling surfaces in ITER and, over the last 6 years, JET has performed a systematic comparison of their merits (eg [1]). Principal considerations relate to the structural properties of the materials, such as thermal conductivity and radiation damage, erosion rates and melting (of beryllium), plasma contamination, and the retention of hydrogen isotopes. In the most recent phase of the JET experiment, the properties of plasmas using CFC and beryllium targets were investigated in the MkI Pumped Divertor (eg [2]). Here the characteristics of L and H-mode plasmas are discussed, and the power handling properties of the targets are described. Companion papers report the results of erosion measurements [3] and of the analysis of hydrogen retention [4].

In the JET MkI Pumped Divertor (Fig.1), the divertor target consisted of water-cooled beams, for inter-pulse cooling, clad in either CFC or beryllium tiles. The former were in place for most of the experimental campaign, while the latter were used during the final two months of experimentation. The tiles forming the power handling surfaces had toroidal widths in the range of 3-4cm and a radial length of ~8cm. The tile surfaces were profiled to avoid exposure of tile edges to plasma incident along field lines, and the front surface of the beryllium tiles was also castellated (with dimensions 8×8mm) to relieve thermal stresses. In addition, the use of strike point sweeping at 4Hz was integral to the design of the MkI power handling capability

and was used, with strike point sweep amplitudes of up to 10cm, in the majority of experiments discussed. It is important to note that CFC is used extensively for first wall protection, as shown in the figure, and this is believed to be a significant source of impurities in JET plasmas. Overnight beryllium evaporation, applying layers of ~10nm, was exploited routinely for vessel conditioning, so that both the CFC and beryllium phases of the experiment suffered from cross-contamination of the other material. Active pumping using a cryopump operating at liquid helium temperatures, and located behind the outer vertical divertor target, was used to provide particle control in all plasmas considered here.

2. CHARACTERISTICS OF L AND H-MODE PLASMAS

A wide range of experiments, in various plasma configurations and using both the horizontal and vertical target plates, was carried out in assessing the relative performance of the targets. The general characteristics of plasmas on the beryllium and CFC targets were very similar. In ohmic, L-mode and H-mode plasmas, radiation levels, the approach to detachment and the density limit were similar. Impurity analysis showed that carbon influxes were perhaps a factor of 2-3 higher on the CFC target, with the carbon yield from the target in the range 1-2% for an H-mode at 10MW. Beryllium influxes were typically a factor of 5-10 higher on the beryllium than on the CFC target, but before the beryllium melt experiment (see Section 4), the beryllium yield was usually below 1%. In general, carbon line radiation, rather than beryllium, appeared to dominate the impurity radiation losses [5]. Carbon was also the dominant contributor to Z_{eff}, which was generally in the region of 1-1.5. Impurities such as oxygen and chlorine contributed only a few percent of the radiated power and the random variation between different phases of the experiment, for example following in-vessel interventions, masked any systematic differences between the carbon and beryllium target phases.

The development of steady-state plasmas in which the majority of the exhaust power is dissipated by radiation and charge exchange processes was an important aspect of the Pumped Divertor experiments (eg [6]). Steady-state detached L-modes in which 70-80% of the input power was lost through radiation were readily established on both targets. If the window for detachment is defined to lie between the 'roll-over' in ion saturation current observed at the target Langmuir probes [7] and the density limit, a similar window was observed for the two target materials. Figure 2 shows the density at which the 'roll-over' and the density limit occurred in plasmas on the CFC and Be targets as a function of power. Results for two plasma configurations are shown: a 'low flux expansion' case, with a flux expansion of ~2 between the plasma midplane and the outer divertor strike point, and a 'high flux expansion case', with a flux expansion ~4. It can be seen that both the 'roll-over' density and the density limit are very similar. In addition, the L-mode density limit was found to be disruptive for both targets. This is in contrast to previous results obtained in limiter experiments [8], where the frequency of

disruptions was considerably reduced following the installation of the beryllium limiter. Whether the difference in behaviour between the limiter and divertor plasmas is due to the dominance of carbon in the latter experiments, or whether the dynamics of the density limit MARFEs differ in the two configurations is unclear. It should also be noted that, in moderate to high density plasmas, fuelling efficiency was similar for CFC and beryllium, an observation which is explained by the dominant role of the divertor cryopump in the particle balance [9].

Steady-state H-modes were explored from 1 to 6MA at total powers of up to 30MW [10]. Their general characteristics, including energy confinement and H-mode power threshold, were again virtually indistinguishable. Steady-state densities were very similar, as was the range of densities attained. Figure 3 compares two steady-state H-modes at 3MA, illustrating the similarity in global characteristics. At the highest densities, plasmas returned to the L-mode when the radiated power fraction was only 40-50%, that is well before divertor detachment occurred. Radiative divertor regimes were established using several impurity gases, but predominantly nitrogen [11]. The properties of these radiating divertor H-modes exhibited little dependence on the target material, and, at radiated power fractions of 80%, energy confinement enhancement factors of 1.6 relative to ITER89-P scaling were achieved.

3. POWER HANDLING CAPABILITY OF THE TARGETS

Particular care was taken in the design and installation of the MkI divertor targets to avoid direct exposure of tile edges to plasma so as to avoid carbon blooms, which had limited the scope of JET experiments in earlier campaigns. A similar approach was taken to the design of the beryllium targets, since surface melting had clearly been recognized as a limiting factor in previous experiments. Careful design, the routine use of strike point sweeping, and the redistribution of power by ELMs in steady-state H-modes combined to limit the surface temperature rise observed, even at deposited energies of 100MJ. In general the temperature of the CFC target rarely exceeded 1200°C [12], and carbon blooms were never observed, even in the high power ELM-free high H-modes used in high fusion performance experiments [13].

Analysis of tile heating data from the beryllium experiment showed that the target surface temperature rose as $(P_{tot}-P_{rad})t^{0.5}$, as expected from the simplest, semi-infinite-solid analysis of power handling. Figure 4 illustrates the observed temperature rise at the outer divertor strike point, measured by an infra-red camera, as a function of $(P_{tot}-P_{rad})t^{0.5}$ in a series of unswept neutral beam heated L-mode discharges with the same magnetic equilibrium. Two fit lines are shown, one calculated on the assumption that the power conducted and convected across the separatrix was shared equally between the inner and outer divertor legs, and the other assuming that all of the conducted power was deposited on the outer strike point. Although the former assumption appears to yield better agreement, this should not be interpreted as demonstrating that the conducted power was shared equally between the two strike points. For example, the

slope of the curves can be varied by changing the assumed value of the outer midplane SOL width - a reasonable, but not exact, assumption of λ~1cm was used. Moreover, the temperature rise at the inner strike point often fell below the camera detection limit of ~300°C, in part due to the higher flux expansion, in part due to the higher radiation losses observed at the inner strike point.

The success of the beryllium target tile design was confirmed by the absence of melting on tile edges. Nevertheless, several individual instances of surface melting with Be did occur in advance of the deliberate melt experiment. The first of these was observed during the initial (unswept) power handling investigations at a measured temperature of ~800°C, indicating that the spatial resolution of the IR camera and uncertainties in the surface emissivity of beryllium limited the accuracy with which the peak temperature could be measured. Additional melt events occurred as a result of singular giant ELMs during high performance and high current experiments. Such an event is illustrated in figure 5. In this case, two ELMs separated by ~200ms each deposited ~1MJ in less than 20ms. the resultant sudden temperature rise of the target is shown in the figure, though the measured temperature was well below the beryllium melting temperature (1270°C) due to the slow time response of the IR camera. Damage to the target tiles was of limited depth (<<1mm) and did not restrict the scope of the programme when swept configurations were used.

In contrast to the damage produced by giant ELMs, there was no evidence of melt damage associated with the energy quench at major disruptions, although very similar energy losses and timescales were involved. Specific experiments were performed to optimize the measurement capability and to ensure that the plasma disrupted in contact with the beryllium target. However, although temperatures of at least 1000°C were detected (with 2ms time resolution), no melt damage could be observed with a camera viewing the target with a spatial resolution of several mm (capable of resolving the melt damage due to giant ELMs). *Post-mortem* examination of the tiles revealed no significant toroidal asymmetries which could be associated with disruptive energy quenches.

Total energies of ~50MJ were deposited on the beryllium target in advance of the melt experiment, a figure limited only by the experimental time available, compared to 100MJ in equivalent plasmas on the CFC target. Experiments were also conducted using the divertor side-plates at total deposited energies of ~20MJ (the comparative figure with CFC was 50MJ). These figures are far superior to those achieved in previous beryllium target experiments.

4. BERYLLIUM MELT EXPERIMENT

A specific experiment was performed to assess the behaviour of the beryllium target at power fluxes high enough to cause surface melting [14]. These experiments were designed to test the speculation that in ITER a beryllium divertor target would self-protect against excessive, off-

normal, heat fluxes (assumed to be ~25MWm^{-2}), for example as might occur when radiative divertor operation fails. In this scenario, a highly radiating region produced by evaporating beryllium would reduce the heat flux to the target, preventing significant melting.

In a series of discharges with additional deuterium puff rates of 2.5×10^{22} electrons/s, the integrated heat flux to the target was gradually increased and beryllium influxes were seen to rise significantly with target temperatures above about 1200°C (Fig. 6). No transition between evaporation of beryllium from the solid surface and influxes from the melt layer could be distinguished. Subsequently, in a series of discharges with gas puffing, the heat flux and the duration of the heating pulse were increased (to ~25MWm^{-2} for ~6s) and significant melting of the target was observed with a CCD in-vessel viewing camera. Nevertheless, the radiated power did not exceed 50% of the input power and ELMy H-mode operation was retained. In a further series of discharges without additional gas-puffing, but at similar heat fluxes and heating duration, the radiated power was observed to rise to ~70% over several seconds. This is the only evidence of self-protection in these experiments. Nevertheless, in this phase of the experiment, melting was observed on both the inner and outer strike points. The total exposure time of the target to the high heat flux was ~20s and no disruptions occurred during the sequence of pulses which melted the target.

After melting, reference plasma scenarios were repeated with strike points on the annuli of melted beryllium. The plasmas investigated included ELMy H-modes, with and without gas puffing, and nitrogen seeded radiative divertor plasmas. These discharges, which were performed without sweeping to maximize the interaction with the damaged area, were only marginally worse than the pre-melt references. Figure 7 compares an (unswept) ELMy H-mode with gas puffing at a rate of ~2.5×10^{22} electrons/s with a similar (swept) case produced before the melting sequence. With the exception of an initial transient rise in the BeII emission at the onset of heating in the post-melt case, the global characteristics of the two discharges are remarkably similar. ELMy H-modes without gas-puffing were more strongly degraded relative to the pre-melt references, although the degradation reduced after a few shots. Finally, two long pulse, high power discharges with sweeping and with total input energies of 120 and 180MJ respectively were performed on a different annulus of the target. Beryllium melting was observed, but the radiated power fraction did not exceed 40%, again indicating that self-protection did not occur.

Post-mortem examination of the target revealed significant droplet formation in the exposed areas, with droplets forming bridges across the 10mm toroidal gaps between the tiles. In the most severely melted regions, an annulus approximately 40mm wide at the outer strike point, tiles were eroded to a depth of about 3mm. The damage exhibited near perfect toroidal symmetry, confirming the excellent installation alignment of the tiles. It can be concluded, therefore, that at heat fluxes of 25MWm^{-2}, severe melting of beryllium occurs. While a certain degree of self-protection was evident, this was insufficient to protect the tiles from melt damage.

Such damage does not prohibit subsequent plasma operation, but may be expected to lead to rapid failure of the component, either by erosion or by fatigue.

5. DISCUSSION AND CONCLUSIONS

No major changes in plasma or divertor performance were observed between discharges using the CFC and beryllium targets. In particular, detachment and H-mode performance were remarkably similar. Thus, there does not appear to be a strong reason, from the divertor physics point of view, to choose one material in preference to another. One caveat which must be made is that carbon radiation was significant in experiments on the beryllium target. Analysis of tiles removed from the target after the experiment confirmed that substantial amounts of carbon had been deposited on the beryllium tiles in the course of the experimental programme [4]. It is likely, therefore, that carbon sputtered from the main chamber walls and redeposited on the divertor target played an important role in beryllium target experiments, an effect which might have been influenced by the open divertor geometry. In addition, the use of beryllium evaporation throughout the campaign conferred some of the known advantages of beryllium, such as oxygen gettering, on the earlier phase of experiments on the CFC target. The experiments reported here do not, therefore, constitute a comparison between carbon dominated and beryllium dominated plasmas, something which could only be achieved by replacing all power handling and protection surfaces by one material or the other.

The good power handling characteristics of the beryllium target allowed a full programme of experiments to be conducted, though singular giant ELMs caused surface melting. A further positive aspect is that although IR measurements made during disruptions found measured target temperature in the vicinity of 1000°C during the energy and current quenches, no disruption-induced melt events have been identified, either by inter-shot inspection of the target or by *post-mortem* analysis. In spite of this broadly positive operational experience with Be, CFC has clear advantages in power handling in the inertially cooled environment of the JET MkI and MkII divertors.

The beryllium melt experiment showed that at heat fluxes of $25MWm^{-2}$, severe melting of beryllium can be expected. Generally, the radiated power fraction in this phase of the experiment remained below 50%, though in plasmas without gas puffing it reached 70%. Nevertheless, there was little evidence for self-protection of the beryllium layer by radiation as the melting temperature was exceeded. However, one surprising result is that the measured BeII emission from the divertor region was 1-2 orders of magnitude below that expected on the basis of the calculated evaporation rates. This is not understood, although the possibilities that there is a force on the escaping beryllium neutrals driving them away from the plasma, or that the processes governing evaporation and melting in the presence of plasma differ from those in the laboratory have been considered. While satisfactory plasma operation was recovered following

the melt experiment, the level of damage observed would eventually lead to component failure. It would be preferable, therefore, in a reactor environment to implement active measures for the protection of beryllium surfaces against off-normal events, rather than to rely on passive self-protection by beryllium radiation.

ACKNOWLEDGEMENTS

The dedication and expertise of the engineering staff who designed and installed the Pumped Divertor and of the scientific teams who conducted the experimental programme are gratefully acknowledged.

REFERENCES

[1] The JET Team (presented by K J Dietz), Plasma Physics and Contr. Fusion **32** 837 (1990).

[2] The JET Team (presented by M Keilhacker), Plasma Physics and Contr. Fusion **37** A3 (1995).

[3] H Y Guo et al, this conference.

[4] J P Coad et al, this conference.

[5] C F Maggi et al, this conference.

[6] The JET Team (presented by D J Campbell), Plasma Physics and Controlled Nuclear Fusion Research (Proc. 15th Int. Conf., Seville, 1994), Vol 1, IAEA, Vienna, 527 (1995).

[7] R D Monk et al, Controlled Fusion and Plasma Physics (Proc. 22nd Euro. Conf., Bournemouth, 1995), **III** 293 (1995).

[8] C G Lowry et al, Controlled Fusion and Plasma Heating (Proc. 17th Euro. Conf., Amsterdam, 1990), **I** 339 (1990).

[9] G Saibene et al, this conference.

[10] R Sartori et al, ibid ref [6] **IV** 141.

[11] The JET Team (presented by G F Matthews), ibid ref [2] A227.

[12] S Clement et al, ibid ref [6] **III** 309.

[13] The JET Team (presented by T T C Jones), ibid ref [2] A359.

[14] B J D Tubbing et al, ibid ref [6] **III** 453.

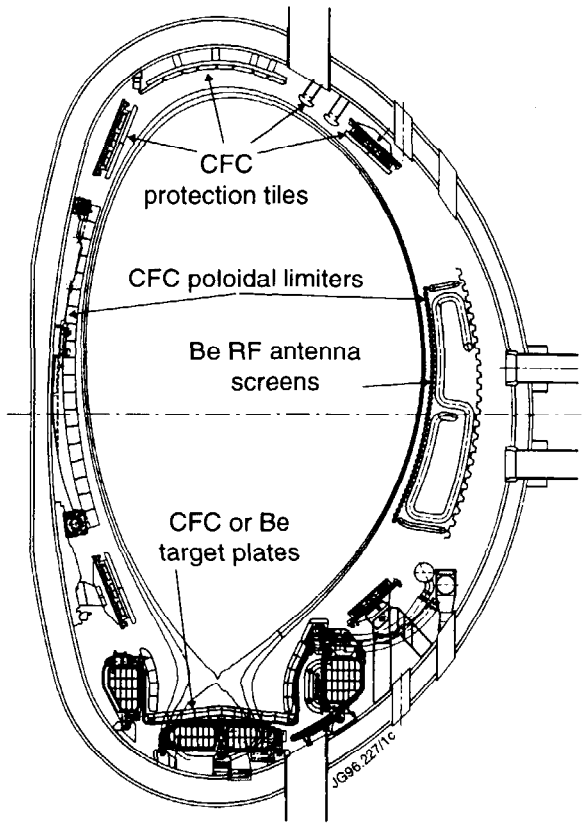

Fig.1: Poloidal cross-section of the JET vacuum vessel for the MkI Pumped Divertor experimental campaign. The main power handling surfaces are indicated. Note also the 4 divertor coils, shown by the cross-hatched regions below and to either side of the divertor target plates, and the divertor cryopump, located in the interspace between the outer vertical target plate and the outermost divertor coil.

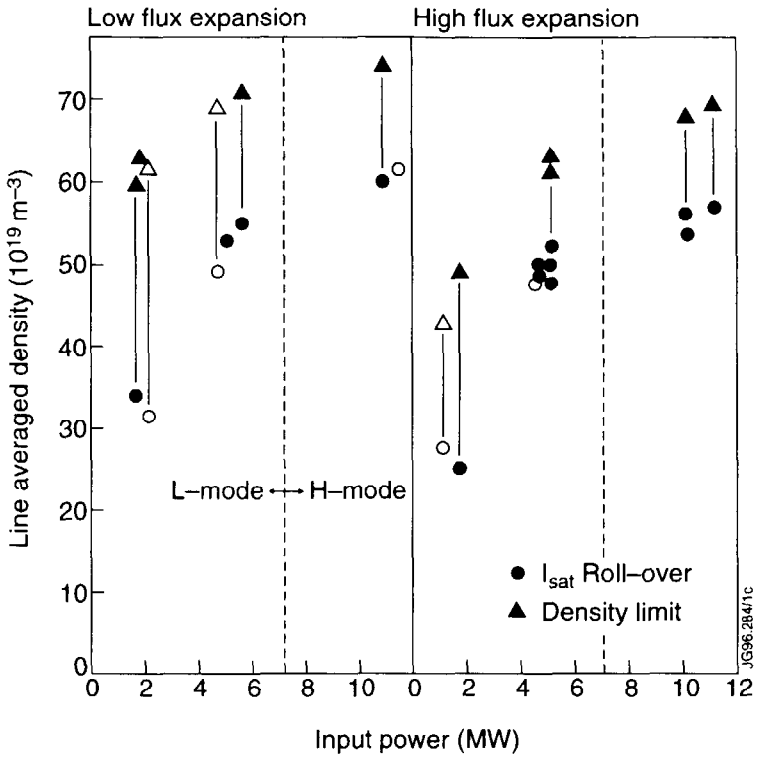

Fig.2: Comparison of the window for detachment for the two divertor targets (solid points for CFC and open points for Be). The density for the onset of the ion saturation current 'rollover' at the target Langmuir probes and the density limit vary in a similar way as the power increases. Results for two different plasma configurations are shown.

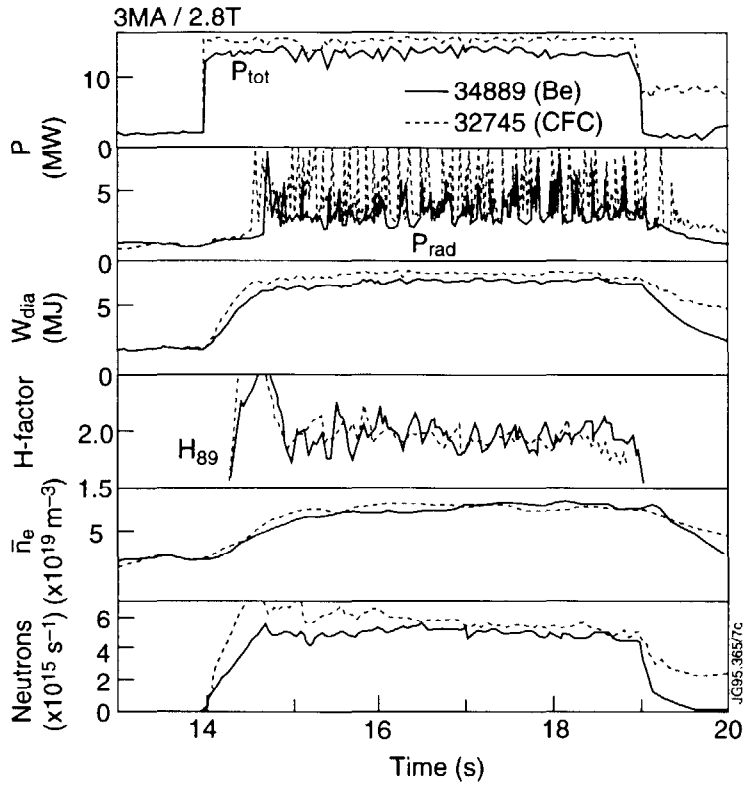

Fig.3: Comparison of the global characteristics of equivalent steady-state H-modes using the CFC and Be targets. Shown are the total input power, P_{tot}, the radiated power, P_{rad}, the H-mode confinement enhancement factor relative to the ITER89-P L-mode scaling, H_{89}, the line averaged plasma density, $\bar{n}_e$, and the neutron yield.

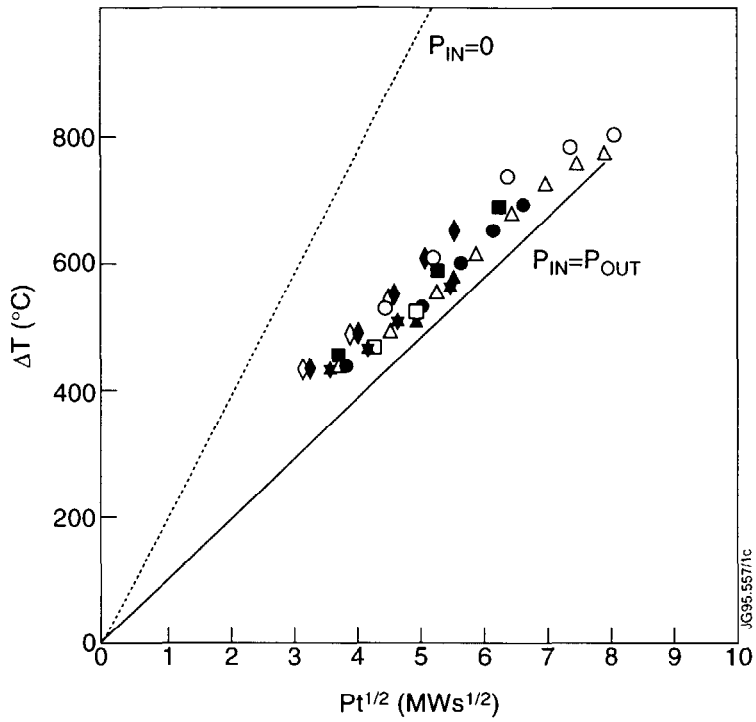

Fig.4: Analysis of the temperature rise at the outer strike point on the beryllium target, measured by an IR camera, plotted against $(P_{tot}-P_{rad})t^{0.5}$ *for a series of NBI heated L-mode plasmas. Two fit curves are shown: the solid assumes that the power conducted and convected across the separatrix is shared equally between the inner and outer divertor legs, while the dashed line assumes that all of the exhaust power flows to the outer strike point. See the text for a discussion of the significance of these assumptions.*

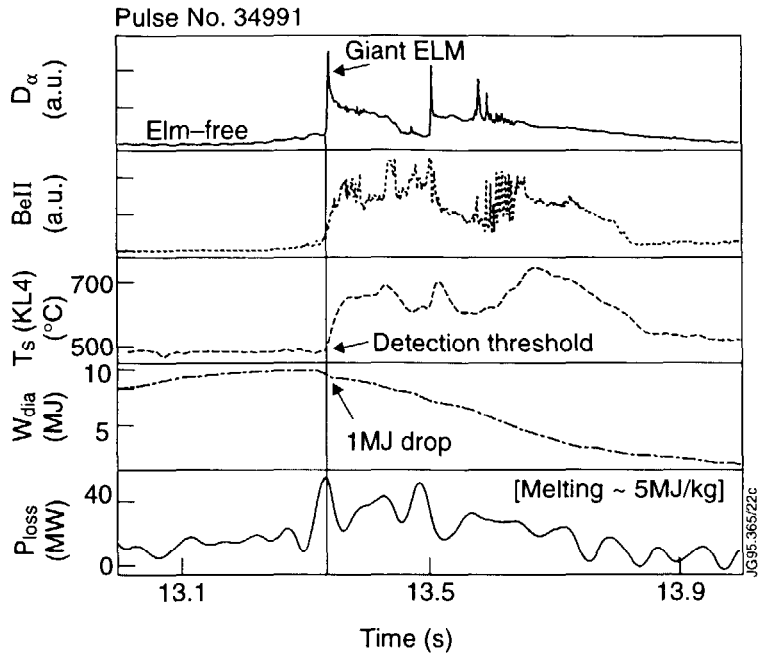

Fig.5: Illustration of a melt event caused by a singular giant ELM which terminated a high performance ELM-free phase. The sudden rise in BeII emission and in the surface temperature of the target, associated with the first giant ELM, are clearly visible. Note that the observed target temperature rise is limited by the time resolution of the IR camera.

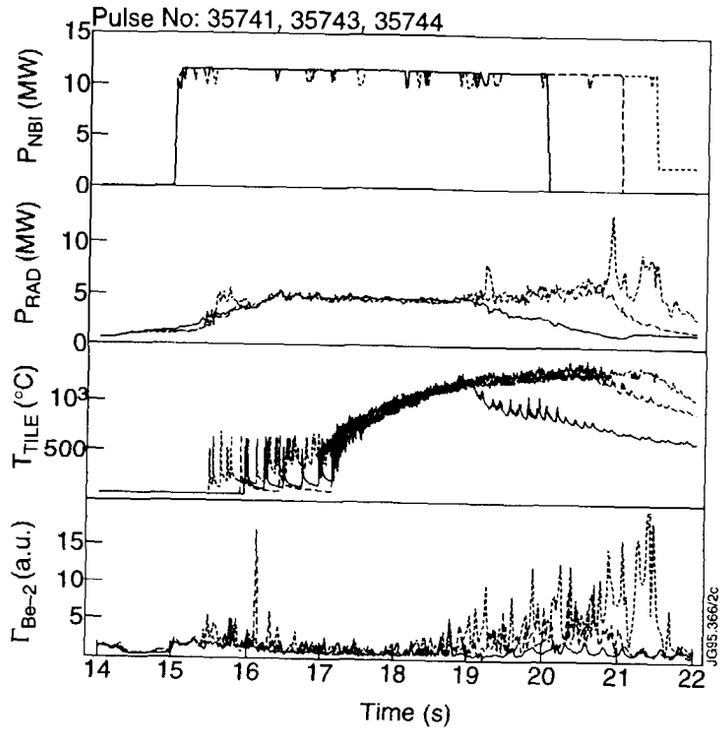

Fig.6: Overview of a series of H-mode discharges, with deuterium puffing at 2.5×10^{22} electrons/s, in which the duration of the unswept heated phase was gradually increased. Shown are the neutral beam input power, P_{NBI}, the radiated power, P_{RAD}, the tile temperature at the outer strike point, T_{TILE}, and the BeII emission, Γ_{Be-2}. The final discharge in the series led to the first visible melting of the target, as indicated by the rise in BeII emission.

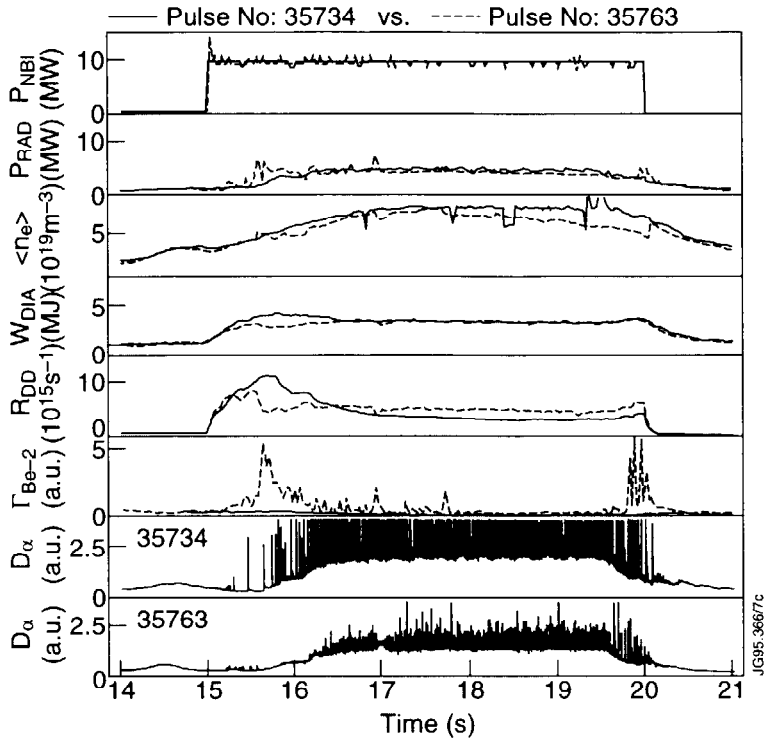

Fig.7: Comparison of ELMy H-modes with deuterium puffing, at 2.5×10^{22} electrons/s, produced before (solid line) and after (dashed line) the melting sequence. Shown are the neutral beam input power, P_{NBI}, the radiated power, P_{RAD}, the tile temperature at the outer strike point, T_{TILE}, the diamagnetic stored energy, W_{DIA}, the DD reaction rate, R_{DD}, the BeII emission, Γ_{Be-2}, and the D_α emission. The overall characteristics of the two discharges are very similar.